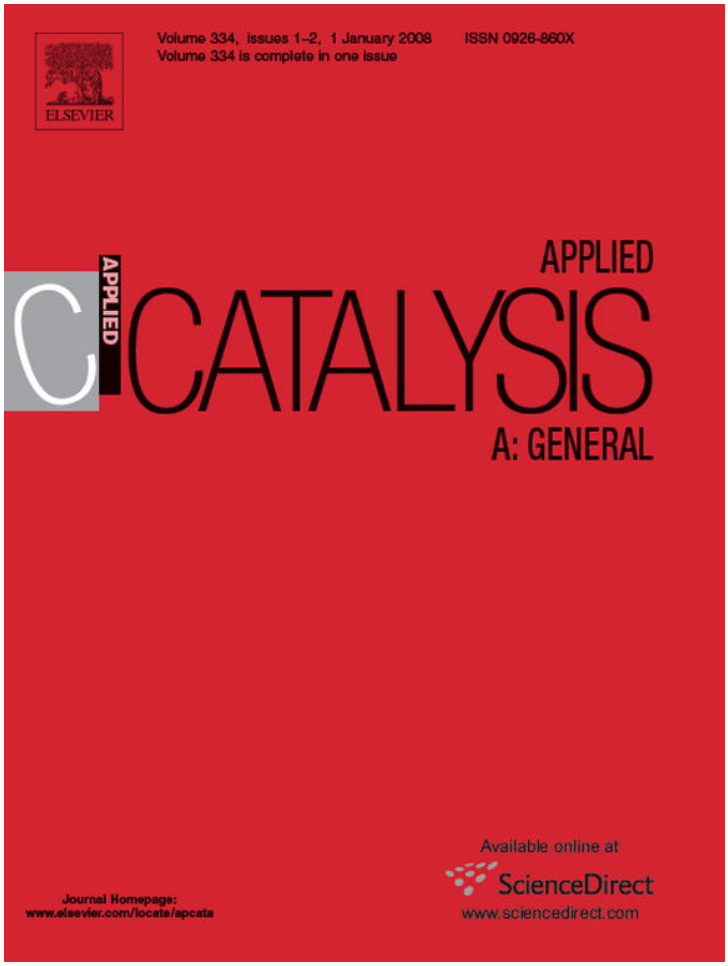

Available online at www.sciencedirect.com
ScienceDirect
Applied Catalysis A: General 334 (2008) 339–347
APPLIED CATALYSIS A: GENERAL
www.elsevier.com/locate/apcata

Support and promoter effects in the selective oxidation of ethane to acetic acid catalyzed by Mo-V-Nb oxides

Xuebing Li, Enrique Iglesia *

Department of Chemical Engineering, University of California, Berkeley, CA 94720-1462, United States

Received 30 August 2007; received in revised form 22 October 2007; accepted 24 October 2007
Available online 30 October 2007

Abstract

Catalysts based on Mo-V-Nb oxides were examined in bulk and supported forms for the oxidation of ethane to ethene and acetic acid. Bulk $Mo_{0.61}V_{0.31}Nb_{0.08}O_x$ powders showed rates and selectivities similar to those in previous reports. Precipitation in the presence of colloidal TiO_2 led to a 10-fold increase in ethene and acetic acid rates (per active oxide) without significant changes in selectivity relative to unsupported samples. Precipitation in the presence of colloidal ZrO_2 and Al_2O_3 suspensions, however, introduced unselective combustion sites without improving ethane oxidation rates. Mo_5O_{14} structures, containing low-valent metal cation centers were detected in bulk $Mo_{0.61}V_{0.31}Nb_{0.08}O_x$ and TiO_2-supported samples by Raman and UV–visible spectra and consistent with X-ray diffraction patterns, but not in Al_2O_3- or ZrO_2-containing catalysts. The introduction of trace amounts of Pd (0.0025–0.01 wt.%), as a physical mixture of separate 0.3 wt.% Pd/SiO_2, led to the near complete depletion of ethene intermediates and to a significant increase in acetic acid synthesis rate. Small PdO_x catalyze ethene oxidation to acetaldehyde, but require the rapid scavenging of these molecules by Mo-V-Nb oxides to prevent acetaldehyde combustion and loss of selectivity. Dispersed VO_x domains on TiO_2 were able to catalyze all steps required for ethane oxidation to acetic acid. CO_x selectivities, however, were much higher than on bulk and TiO_2-supported $Mo_{0.61}V_{0.31}Nb_{0.08}O_x$ catalysts. Dispersed MoO_x domains were essentially inactive at these reaction conditions but their concurrent presence with VO_x increased acetic acid selectivity by titrating unselective sites and stabilizing more reducible VO_x species.

Keywords: Ethane; Oxidation; Metal oxide; Ethene; Acetic acid

1. Introduction

Methanol carbonylation catalyzed by Rh and Ir organometallic complexes (BP-Monsanto Cativa process) and iodide as co-catalysts is the most widely practiced approach for the synthesis of acetic acid [1]. The presence of toxic and corrosive iodide species, the use of expensive and difficult to recover noble metals, and the high CO partial pressures required have led to a search for alternate routes. The synthesis of acetic acid via selective oxidation of ethane [2], ethene [3,4] or ethanol [5–8] on metal oxide domains provides such alternate routes.

Selective oxidation of ethane to ethene and acetic acid was reported by Thorsteinson et al. [2] on mixed metal oxide catalysts containing Mo, V, and another element (Nb, Sb, Ti, Ta, Sn, As, W, Fe) at relatively high pressures (0.5–2.0 MPa) and temperatures (550–600 K). Vanadium phosphate catalysts (VPO), typically used for butane oxidation to maleic anhydride, also form acetic acid from ethane [9–12], but with significant selectivity to CO_x byproducts. Polyoxometallate clusters act as mere precursors for ethane oxidation catalysts, because they decompose to ill-defined mixed oxides at the temperatures and pressures required for practical acetic acid yields from ethane oxidation, and give low acetic acid productivities (<100 g/kg-cat-h) [13,14]. Partially decomposed molybdovanadophosphoric acid clusters exchanged with pyridine also catalyze ethane oxidation to acetic acid albeit with relatively low rates and yields [15,16]. A summary of these previous studies is included in Table 1.

The simple synthetic protocols, high acetic acid yields, and excellent stability of mixed Mo-V-Nb oxides have led to several previous publications and patents. The co-precipitation of noble metals (e.g., Re [17], Pd [18,19]) with Mo-V-Nb oxides increased acetic acid synthesis rates and shifted ethene selectivities towards acetic acid. Previous attempts at supporting Mo-V-Nb oxides on α-Al_2O_3 [2,20] and on SiO_2-TiO_2 [21]

* Corresponding author.
E-mail address: iglesia@berkeley.edu (E. Iglesia).

0926-860X/$ – see front matter © 2007 Elsevier B.V. All rights reserved.
doi:10.1016/j.apcata.2007.10.021

Table 1
Summary of previous publications and present work describing ethane oxidation to acetic acid

Catalyst	T (K)	Ethane con. (%)	Selectivity (%)			Synthesis Rate (g/kg-cat-h)		Reference
			Ethene	Acetic acid	CO_x	Ethene	Acetic acid	
$Mo_{0.77}V_{0.19}Nb_{0.04}O_x$	573	3.7	70	23	7	224	190	[2]
VPO/TiO_2	548	3.2	8	21	71	1	4	[9,10]
VPO/TiO_2	523	1.0	18	36	46	6	26	[11]
$Mo_{0.2}V_1P_{1.15}$	548	1.4	50	31	19	20	27	[12]
$HPMoV_2/TiO_2$	573	6.3	28	12	60	3	3	[13]
$H_6PMo_9V_3O_{40}$	523	0.6	17	78	5	3	27	[14]
$NbPMo_{11}Vpyr$	653	5.7	59	13	28	49	53	[15,16]
$Mo_{37}Re_{25}V_{26}Nb_7Sb_3Ca_2$	550	14.3	12	78	10	8	114	[17]
$Mo_1V_{0.398}La_{7.08e\text{-}6}Pd_{0.0003}Nb_{0.125}Al_{0.226}$	553	10.7	–	–	–	–	310	[18]
$Mo_1V_{0.55}Nb_{0.09}Sb_{0.01}Ca_{0.01}Pd_{0.00075}$	573	13.0	11	81	8	10	410	[19]
50% $Mo_1V_{0.529}Nb_{0.124}Au_{0.0012}$/α-alumina	571	7.0	60	32	8	56	65	[20]
50% $Mo_1V_{0.529}Nb_{0.124}/SiO_2$-$TiO_2$	588	5.0	23	53	24	48	234	[21]
$Mo_{0.61}V_{0.31}Nb_{0.08}O_x/TiO_2$	573	5.4	58	35	7	310	407	This work
0.01% $Pd/Mo_{0.61}V_{0.31}Nb_{0.08}O_x/TiO_2$	573	5.1	1	82	17	4	829	This work

were unsuccessful at increasing the surface area of the active phase or increasing acetic acid productivities over those observed on bulk mixed oxide catalysts (Table 1).

Here, we report Mo-V-Nb oxide catalysts structurally promoted by introducing titania during precipitation. These materials give unprecedented acetic acid synthesis rates when promoted with trace amounts of Pd, present as a physical mixture in the form of a separately prepared Pd/SiO_2 catalyst. Even after many studies, the compositional and structural complexity of bulk Mo-V-Nb oxides has prevented the unequivocal elucidation of the specific function of each component in these oxidation catalysts. In view of this, we also examine here the specific functions of Mo and V components present as dispersed MoO_x and VO_x and their mixtures on various supports. We find that dispersed VO_x domains can activate ethane and convert it to acetic acid, while MoO_x by itself is essentially unreactive.

2. Experimental

2.1. Catalyst synthesis

2.1.1. Synthesis of mixed Mo-V-Nb oxides ($Mo_{0.61}V_{0.31}Nb_{0.08}O_x$)

$Mo_{0.61}V_{0.31}Nb_{0.08}O_x$ powders were prepared using a slurry method [2]. A solution containing $C_4O_8NbOH{\cdot}NH_3$ (ammonium niobate(V) oxalate hydrate; 2.42 g; Aldrich; 99.99%) was added drop-wise to another solution containing $C_2O_4H_2$ (oxalic acid; 7.2 g; Fluka, 99%), NH_4VO_3 (ammonium (meta)vanadate; 3.63 g; Sigma–Aldrich, 99%) and $(NH_4)_6Mo_7O_{24}{\cdot}4H_2O$ (ammonium heptamolybdate tetrahydrate; 10.77 g; Aldrich, 99.98%) at ambient temperature while stirring. The water was then evaporated at 363 K while stirring under dynamic vacuum. The powders formed were treated at 393 K overnight in ambient air and then in flowing dry air (Praxair, extra dry, 1.67 $cm^3\ s^{-1}$) at 673 K for 4 h. This catalyst is denoted herein as $Mo_{0.61}V_{0.31}Nb_{0.08}O_x$.

2.1.2. Synthesis of mixed Mo-V-Nb oxides in the presence of alumina, titania, or zirconia

Three supports were used during precipitation of $MoVNbO_x$ mixed oxides: γ-alumina (Sasol, Puralox, Nwa 155, BET area: 148 $m^2\ g^{-1}$), titania (Degussa, P25, BET area: 49 $m^2\ g^{-1}$) and high-surface area zirconium oxyhydroxide ($ZrO(OH)_2$, BET area: 378 $m^2\ g^{-1}$). The latter was precipitated from a solution containing zirconyl chloride (99.5%, Riedel-de Haën), introduced at 500 $cm^3\ h^{-1}$ into a stirred beaker at a constant pH of 10, held constant by the concurrent addition of ammonium hydroxide (29.8%, Fisher Sci., Inc.). The oxyhydroxide precipitate was filtered and washed with de-ionized water until Cl ions were no longer detected in the filtrate using silver nitrate. The resulting solids were dried overnight in ambient air at 393 K [22].

The support (10 g) was added to a solution containing $C_2O_4H_2$ (oxalic acid; 1.8 g; Fluka, 99%), NH_4VO_3 (ammonium (meta)vanadate; 0.91 g; Sigma–Aldrich, 99%) and $(NH_4)_6Mo_7O_{24}{\cdot}4H_2O$ (ammonium heptamolybdate tetrahydrate; 2.7 g; Aldrich, 99.98%) while stirring at ambient temperature; A $C_4O_8NbOH{\cdot}NH_3$ (ammonium niobate(V) oxalate hydrate; 0.61 g; Aldrich; 99.99%) solution was added drop-wise into the above suspension while stirring at ambient temperature. Water was then evaporated in dynamic vacuum while stirring at 363 K. The resulting powders were dried at 393 K overnight in ambient air and treated in flowing dry air (Praxair, extra dry, 1.67 $cm^3\ s^{-1}$) at 673 K for 4 h. These catalysts are denoted as $Mo_{0.61}V_{0.31}Nb_{0.08}O_x/TiO_2$, $Mo_{0.61}V_{0.31}Nb_{0.08}O_x/Al_2O_3$ and $Mo_{0.61}V_{0.31}Nb_{0.08}O_x/ZrO_2$. The nominal $Mo_{0.61}V_{0.31}Nb_{0.08}O_x$ content was 24 wt.% in all samples.

2.1.3. Synthesis of Pd-containing catalysts

A 0.3 wt.% Pd/SiO_2 sample was prepared by suspending silica (Cab-O-Sil, 99.8%) in an aqueous solution of $[Pd(NH_3)_4](NO_3)_2$ (0.2 wt.%; tetraamminepalladium(II) nitrate; Aldrich, 99.99%) and evaporating the liquid in dynamic vacuum at 363 K while stirring. The resulting solids were dried at 393 K

overnight and treated in flowing dry air (Praxair, extra dry, 1.67 $cm^3\ s^{-1}$) at 773 K for 4 h. Physical mixtures of 0.3 wt.% Pd/SiO_2 and Mo-V-Nb oxide catalysts were prepared by grinding mixed powders with an agate mortar and pestle and then pressing into wafers and sieving to the desired size.

2.1.4. Synthesis of dispersed VO_x, MoO_x and VO_x-MoO_x domains

Dispersed VO_x, MoO_x, and VO_x-MoO_x domains were deposited onto TiO_2 supports in an effort to discern the specific roles of VO_x and MoO_x oxides in $Mo_{0.61}V_{0.31}Nb_{0.08}O_x$ catalysts [23]. TiO_2 was treated in flowing He (Praxair, 99.999%, 1.67 $cm^3\ s^{-1}$) at 573 K for 4 h to remove moisture and suspended in toluene (Aldrich, 99.8%) solutions of vanadyl isopropoxide (Aldrich, 98%) or molybdenyl acetylacetonate (Alfa Aesar, 99%) to form dispersed VO_x or MoO_x structures. The surface densities (8 V nm^{-2} [24] and 5 Mo nm^{-2} [25]) used led to the predominant formation of monomers and two-dimensional metal-oxo oligomers, as confirmed by their Raman spectra. Samples were then treated in flowing dry air (Praxair, extra dry, 1.67 $cm^3\ s^{-1}$) at 673 K for 4 h after removing toluene by evaporation in dynamic vacuum at 363 K. Mixed MoO_x-VO_x samples were prepared by suspending the supported VO_x sample described above in a toluene solution of molybdenyl acetylacetonate and then treating the sample in flowing dry air (Praxair, extra dry, 1.67 $cm^3\ s^{-1}$) at 673 K for 4 h after removing toluene by evaporation in dynamic vacuum at 363 K. These catalysts are denoted here as VO_x/TiO_2 (6.1 wt.% VO_x; 9.0 V nm^{-2}), MoO_x/TiO_2 (5.3 wt.% MoO_x; 4.8 Mo nm^{-2}), MoO_x-VO_x/TiO_2 (2.7 wt.% MoO_x; 3.1 wt.% VO_x; 4.5 V nm^{-2}; 2.4 Mo nm^{-2}).

2.2. Structural and textural characterization

BET surface areas and pore size distributions were measured using a Quantasorb apparatus (Quantasorb 6 Surface Analyzers, Quantachrome Corp.) using N_2 at its normal boiling point. Samples were treated in dynamic vacuum (0.1 Pa) at 398 K overnight before BET measurements. X-ray diffraction (XRD) patterns were measured with a Siemens D5000 diffractometer using Cu-Kα radiation and a scan rate of 1.2° min^{-1}.

A Hololab Series 5000 spectrometer (Kaiser Optical) equipped with a frequency-doubled 75-mW Nd-YAG laser (532 nm) was used to measure Raman spectra. Self-supported wafers (0.9 cm diameter) were placed on a rotating holder within a quartz cell and treated in flowing dry air (Airgas, zero grade, 0.83 $cm^3\ s^{-1}$) at 673 K for 2 h and cooled to ambient temperature before acquiring spectra.

Diffuse-reflectance UV–vis spectra were collected with a Cary 4 spectrophotometer (Varian Corp.) equipped with an *in situ* flow cell (Harrick) and a diffuse reflectance accessory. Samples were treated in a mixture of O_2 (Praxair, 99.999%, 0.08 $cm^3\ s^{-1}$) and He (Praxair, 99.999%, 0.58 $cm^3\ s^{-1}$) at 673 K for 2 h before acquiring reflectance spectra, which were converted into pseudo-absorbances using the Kubelka–Munk formalism ($F(R_\infty)$) and MgO as a reflective standard. The *x*-intercept of a linear regression of $[(F(R_\infty))h\nu]^{1/2}$ measurements as a function of $h\nu$ was used to determine absorption edge energies using procedures previously reported [26].

Exposed support surfaces were determined by chemisorption of CO_2 at 313 K [26,27] using a Quantachrome 1C Autosorb apparatus. Adsorbed H_2O and CO_2 were removed before CO_2 uptake measurements by treating samples (~0.1 g) in He as the temperature was increased to 673 K at 0.083 K s^{-1} and held for 2 h. Samples were then cooled to 313 K and CO_2 adsorption isotherms were measured at 5–75 kPa CO_2 (Praxair, 99.998%). Saturation chemisorption uptakes were determined by extrapolating uptakes to zero CO_2 pressure.

2.3. Ethane oxidation rates and selectivities

Ethane oxidation rates and selectivities were measured using a stainless steel tubular reactor (10 mm inner diameter). The temperature was measured with a K-type thermocouple (Omega, 0.05 cm diameter, 46 cm length) located within a concentric axial thermowell. Reactant mixtures consisted of ethane 33%, O_2 6.67%, H_2O 20%, He 40% and N_2 0.67%. The inlet molar rates of ethane (Praxair, 99.999%), He (Praxair, 99.999%) and N_2/O_2 (Praxair mixture, 10% N_2 in O_2, certified) were metered by electronic controllers (Porter Inc.). H_2O (de-ionized, resistivity: >18.0 MΩ cm) was added to the reactant mixture using a high-pressure syringe pump (Teledyne Isco Inc., model: 500 D). All lines, valves and pressure regulators were kept above 433 K to avoid condensation of water or acetic acid. Reaction rates were measured at 573 K and 1.6 MPa total pressure; the system pressure was measured with a mechanical pressure gauge (Matheson Inc.).

Catalyst pellets (0.25–0.50 mm diameter; 0.2–1 g) were diluted with acid-washed quartz of similar size (Aldrich, White Quartz, 2–2.8 g to give a total bed weight of 3 g) and treated in a mixture of He (Praxair, 99.999%, 0.49 $cm^3\ s^{-1}$) and N_2/O_2 (Praxair mixture, 10% N_2 in O_2, certified, 0.09 $cm^3\ s^{-1}$) at 673 K for 2 h. Ethane and O_2 conversion levels were varied by changing the flow rate of reactants (0.25–4.0 $cm^3\ s^{-1}$) at constant temperature and reactant pressures.

Reactant and product concentrations were measured by direct sampling of flowing streams into a gas chromatograph (Hewlett-Packard 5890, II) equipped with flame ionization and thermal conductivity detectors. N_2, O_2, CO, CO_2 and H_2O were separated with a Plot Q capillary column (HP; 30 m × 0.32 mm) and ethane, ethene and acetic acid were separated with a Plot U capillary column (HP; 30 m × 0.32 mm).

3. Results and discussion

3.1. Catalyst characterization

Measured surface areas and VO_x surface densities (calculated from V contents and BET areas) are shown in Table 2. $Mo_{0.61}V_{0.31}Nb_{0.08}O_x$ gave modest surface areas (7.8 $m^2\ g^{-1}$), suggesting that only a small fraction of the active components are accessible to reactants.

γ-Al_2O_3 and $ZrO(OH)_2$ supports have surface areas of 148 and 378 $m^2\ g^{-1}$, respectively and TiO_2 has a surface area of

Table 2
BET surface areas and VO_x surface density

Catalyst	V_2O_5 (wt.%)	Surface area (m^2 g-cat^{-1})/(m^2 g-support^{-1})	VO_x surface density (V nm^{-2})
Al_2O_3 (Sasol, NWa 155)	0	148	0
TiO_2 (Degussa, P25)	0	49	0
$ZrO(OH)_2$	0	378	0
$Mo_{0.61}V_{0.31}Nb_{0.08}O_x$	31	7.8	263
$Mo_{0.61}V_{0.31}Nb_{0.08}O_x/TiO_2$	7	34 (42)	14.5
$Mo_{0.61}V_{0.31}Nb_{0.08}O_x/Al_2O_3$	7	136 (170)	3.6
$Mo_{0.61}V_{0.31}Nb_{0.08}O_x/ZrO_2$	7	260 (322)	1.9
VO_x/TiO_2	6.1	44 (47)	9.0

49 m^2 g^{-1}. Surface areas for all supported samples were slightly smaller than for the fresh supports, but only because of the additional mass of the active components. Surface areas per mass of support were the same in supported samples and in the corresponding fresh supports (Table 2). VO_x surface densities in dispersed VO_x catalysts are similar to those required for the formation of polyvanadate monolayers (8 V nm^{-2} [24]).

Fig. 1 shows X-ray diffraction patterns for $Mo_{0.61}V_{0.31}Nb_{0.08}O_x$ and $Mo_{0.61}V_{0.31}Nb_{0.08}O_x/TiO_2$. XRD patterns for the bulk samples resemble those reported previously for similarly prepared bulk samples [2], with a strong line at a 2θ value of 22.5° and weaker lines at 25–30°. These lines have been assigned to Mo_5O_{14}-like structures formed when V or Nb substitute into Mo_5O_{14} [28]. $Mo_{0.61}V_{0.31}Nb_{0.08}O_x/TiO_2$ gave strong lines for the anatase and rutile forms of the TiO_2 support and a weak line at 22.5° for Mo_5O_{14}-like structures. The latter feature is not evident in the patterns for $Mo_{0.61}V_{0.31}Nb_{0.08}O_x/ZrO_2$ and $Mo_{0.61}V_{0.31}Nb_{0.08}O_x/Al_2O_3$, indicating that active oxide structures ZrO_2 and Al_2O_3 supports differ from those on bulk or TiO_2-supported samples.

Fig. 2 shows Raman spectra for $Mo_{0.61}V_{0.31}Nb_{0.08}O_x$ and $Mo_{0.61}V_{0.31}Nb_{0.08}O_x/TiO_2$ at ambient temperature, after treatment in flowing dry air at 673 K for 2 h. Raman spectra for $Mo_{0.61}V_{0.31}Nb_{0.08}O_x$ indicate the presence of Mo_5O_{14}-type structures, which exhibit a broad band at 884 cm^{-1} [29]. These Mo_5O_{14} type structures are metastable towards decomposition to MoO_2 and MoO_3 crystalline structures [30,31]. The weak Raman band at 828 cm^{-1} is assigned to trace amounts of α-MoO_3, while the broad band at 711 cm^{-1} corresponds to crystalline V_2O_5 [32]. The spectrum for $Mo_{0.61}V_{0.31}Nb_{0.08}O_x/TiO_2$ shows the presence of Mo_5O_{14}-type structures, with a weak band at 884 cm^{-1} and a spectrum dominated by the strong bands for crystalline TiO_2 (149, 400, 520, and 644 cm^{-1}). Raman bands for VO_x domains on TiO_2 at 1040 cm^{-1} were assigned to V=O stretches in monovanadates and polyvanadates (Fig. 2) [33,34]. No Raman bands for crystalline V_2O_5 were detectable (1006, 711, 537, 493, 415, 311, 294, 204, 154 cm^{-1}), indicating that VO_x domains exist predominantly as monovanadates and polyvanadates in such samples.

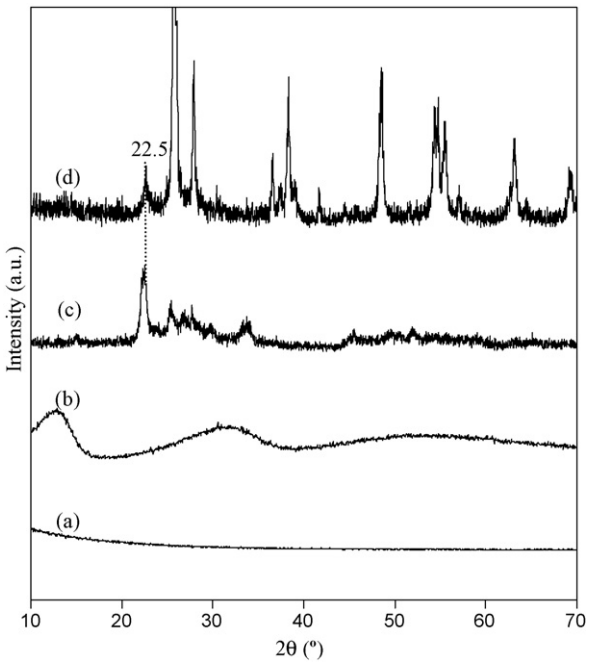

Fig. 1. XRD patterns of (a) $Mo_{0.61}V_{0.31}Nb_{0.08}O_x/Al_2O_3$, (b) $Mo_{0.61}V_{0.31}Nb_{0.08}O_x/ZrO_2$, (c) $Mo_{0.61}V_{0.31}Nb_{0.08}O_x$, and (d) $Mo_{0.61}V_{0.31}Nb_{0.08}O_x/TiO_2$.

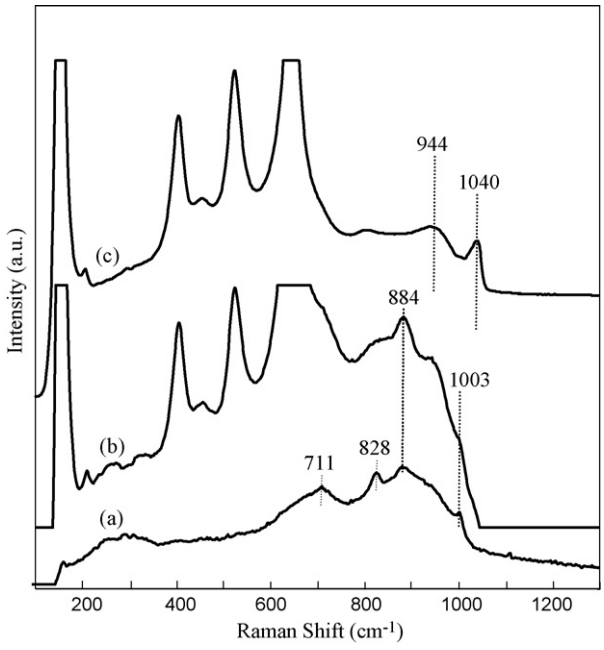

Fig. 2. Raman Spectra of (a) $Mo_{0.61}V_{0.31}Nb_{0.08}O_x$, (b) $Mo_{0.61}V_{0.31}Nb_{0.08}O_x/TiO_2$ and (c) VO_x/TiO_2. Spectra were collected at ambient temperature after samples were treated in flowing dry air at 673 K for 2 h.

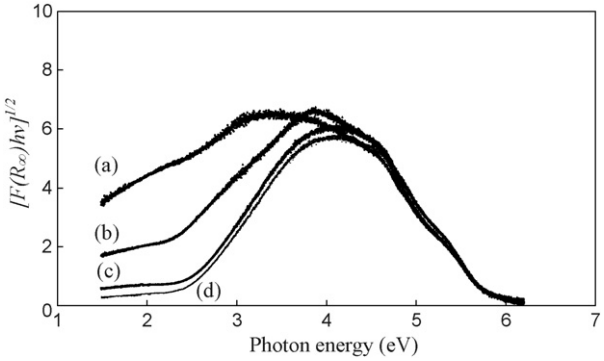

Fig. 3. UV–vis spectra of (a) $Mo_{0.61}V_{0.31}Nb_{0.08}O_x$, (b) $Mo_{0.61}V_{0.31}Nb_{0.08}O_x/TiO_2$, (c) $Mo_{0.61}V_{0.31}Nb_{0.08}O_x/Al_2O_3$ and (d) $Mo_{0.61}V_{0.31}Nb_{0.08}O_x/ZrO_2$. Spectra were collected at ambient temperature after samples were treated at 673 K in flowing He and O_2 for 2 h.

Fig. 3 shows UV–vis spectra for $Mo_{0.61}V_{0.31}Nb_{0.08}O_x$ and $Mo_{0.61}V_{0.31}Nb_{0.08}O_x$ supported on TiO_2, Al_2O_3 or ZrO_2. $Mo_{0.61}V_{0.31}Nb_{0.08}O_x$ showed absorption features at energies below its absorption edge, indicative of d–d transitions in reduced V or Mo centers [23] and consistent with the presence of Mo^{4+} atoms in Mo_5O_{14} structures. TiO_2-supported samples showed weaker pre-edge features than bulk mixed oxides; while oxides supported on Al_2O_3 or ZrO_2 did not show detectable pre-edge absorption features, suggesting that Mo_5O_{14}-like structures were not present in latter two samples. The color of bulk and TiO_2-supported samples is consistent with the presence of low-valent metal cations, which typically give stronger absorption and darker colors than elements in their highest oxidation state. $Mo_{0.61}V_{0.31}Nb_{0.08}O_x$ is typically dark grey, but becomes dark green when supported on TiO_2 and yellow when supported on Al_2O_3 or ZrO_2.

CO_2 chemisorption uptakes were used to measure the exposed support surfaces by comparing uptakes on samples with and without active oxides. Table 3 shows these data and the fraction of the support surfaces covered by the active oxides. The low CO_2 uptake on supported samples shows that >80% of the support is covered by well-dispersed active oxides.

Table 3
Coverage of support by CO_2 chemisorption

Catalyst	CO_2 uptake (CO_2 nm^{-2})	Support coverage (%)
Al_2O_3 (Sasol, NWa 155)	0.44	0
TiO_2 (Degussa, P25)	0.50	0
$ZrO(OH)_2$	0.72	0
$Mo_{0.61}V_{0.31}Nb_{0.08}O_x/Al_2O_3$	0.01	99
$Mo_{0.61}V_{0.31}Nb_{0.08}O_x/TiO_2$	0.09	82
$Mo_{0.61}V_{0.31}Nb_{0.08}O_x/ZrO_2$	0.07	90
VO_x/TiO_2	0.07	86

3.2. Ethane oxidation to ethene and acetic acid on bulk $Mo_{0.61}V_{0.31}Nb_{0.08}O_x$ catalysts

Bulk $Mo_{0.61}V_{0.31}Nb_{0.08}O_x$ catalysts gave 25–32% acetic acid selectivity and 63–73% ethene selectivity at ethane conversions between 0.5 and 6% at 573 K (Fig. 4). Ethane conversion and acetic acid synthesis rates were 0.60–0.77 $\times 10^{-3}$ and 0.15–0.25 $\times 10^{-3}$ mol g-atom-V^{-1} s^{-1} in this conversion range and decreased slightly with increasing residence time. These selectivities resemble those reported previously on catalysts prepared similarly (24% acetic acid; 70% ethene, 3.7% ethane conversion) [2].

Ethane conversion levels were varied by changing space velocity (SV; cm^3-ethane g-$V_2O_5^{-1}$ h^{-1}) to probe the relative contributions of primary and secondary reaction pathways to ethene, acetic acid, and CO_x synthesis. Acetic acid selectivities increased slightly with residence time (1/SV) (from 25 to 32%), while ethene selectivity concurrently decreased (from 73 to 63%), consistent with the involvement of ethene as a reactive intermediate in acetic acid synthesis [35]. The non-zero acetic acid selectivity, evident by extrapolation to zero residence time (Fig. 4), suggests, however, that a substantial fraction of the acetic acid forms via direct oxidation of ethane [36]. The slight decrease in ethane conversion rates (from 0.77 to 0.60 $\times 10^{-3}$ mol g-atom-V^{-1} s^{-1}) and acetic acid synthesis rates (from 0.24 to 0.18 $\times 10^{-3}$ mol g-atom-V^{-1} s^{-1}) observed with increasing residence time (1/SV; from 0.074 to 1.19 g-V_2O_5 h cm^{-3}-ethane) and ethane conversion (from 0.5 to 6.4%) reflects weak inhibition effects by ethene, acetic acid or

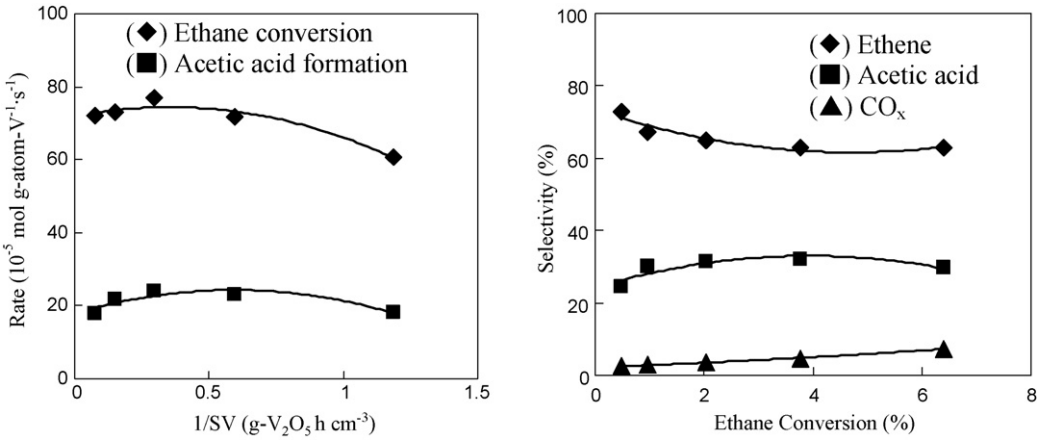

Fig. 4. Ethane oxidation on $Mo_{0.61}V_{0.31}Nb_{0.08}O_x$ at 573 K. Partial pressures: ethane, 533 kPa; O_2, 107 kPa; H_2O, 320 kPa; He, 629 kPa; N_2, 11 kPa.

CO_x products, but not by water, which is present in the inlet stream at high partial pressures (320 kPa).

3.3. Support effects on acetic acid synthesis catalyzed by supported $Mo_{0.61}V_{0.31}Nb_{0.08}O_x$

The low surface area of unsupported $Mo_{0.61}V_{0.31}Nb_{0.08}O_x$ catalysts ($7.8\ m^2\ g^{-1}$) led us to consider potential rate improvements by precipitating these structures in the presence of colloidal dispersions of inorganic oxides with much higher surface areas (e.g., γ-alumina ($148\ m^2\ g^{-1}$), titania ($49\ m^2\ g^{-1}$), or zirconia ($378\ m^2\ g^{-1}$)).

Fig. 5 shows ethane oxidation rates on supported and unsupported $Mo_{0.61}V_{0.31}Nb_{0.08}O_x$ catalysts as a function of residence time. Product selectivities are shown as a function of ethane conversion, varied by changing residence time. $Mo_{0.61}V_{0.31}Nb_{0.08}O_x$ species formed in the presence of a colloidal dispersion of TiO_2 gave much higher acetic acid synthesis rates (9.0×10^{-3} mol g-atom-V^{-1} s^{-1}) than on $Mo_{0.61}V_{0.31}Nb_{0.08}O_x$ powders (0.77×10^{-3} mol g-atom-V^{-1} s^{-1}) without any detectable effects on selectivities (50–60% ethene; 35–40% acetic acid). Ethene selectivities decreased slightly with increasing contact time, as a result of its subsequent conversion to acetic acid and CO_x, while acetic acid selectivities remained relatively constant because of a balance between its formation and its secondary conversion to CO_x, as also observed on $Mo_{0.61}V_{0.31}Nb_{0.08}O_x$ powders. Thus, the structures formed during precipitation in the presence and absence of TiO_2 show similar reactive properties, but appear to have a higher surface area exposed to ethane reactants.

The surface area of the $Mo_{0.61}V_{0.31}Nb_{0.08}O_x/TiO_2$ catalysts is $34\ m^2\ g^{-1}$, but part of these exposed surfaces may consist of unreactive exposed TiO_2, left uncovered by the precipitation process. We measured the uptakes of CO_2, which selectively titrate TiO_2 surfaces [26,27], to determine contributions from exposed TiO_2 to measured BET areas. CO_2 chemisorption at 313 K (by extrapolation to zero pressure) showed that ~82% of the TiO_2 surface was covered ($0.50\ CO_2\ nm^{-2}$ on TiO_2; $0.09\ CO_2\ nm^{-2}$ on $Mo_{0.61}V_{0.31}Nb_{0.08}O_x/TiO_2$). Thus, active $Mo_{0.61}V_{0.31}Nb_{0.08}O_x$ components have a surface area of ~$28\ m^2\ g^{-1}$, about three times larger than the case of unsupported $Mo_{0.61}V_{0.31}Nb_{0.08}O_x$ catalysts ($7.8\ m^2\ g^{-1}$).

These active component areas can be used to calculate areal ethane conversion rates and acetic acid synthesis rates on $Mo_{0.61}V_{0.31}Nb_{0.08}O_x/TiO_2$ (1.9×10^{-7} mol s^{-1} m^{-2}) and $Mo_{0.61}V_{0.31}Nb_{0.08}O_x$ (2.2×10^{-7} mol s^{-1} m^{-2}) catalysts. We conclude from these data that the higher rates (per V-atom) on TiO_2-containing catalysts merely reflect a higher dispersion of the active Mo-V-Nb oxide species, without detectable changes in their intrinsic reactivity or selectivity. The structural similarity of the active components in unsupported and TiO_2-containing catalysts was confirmed by their similar

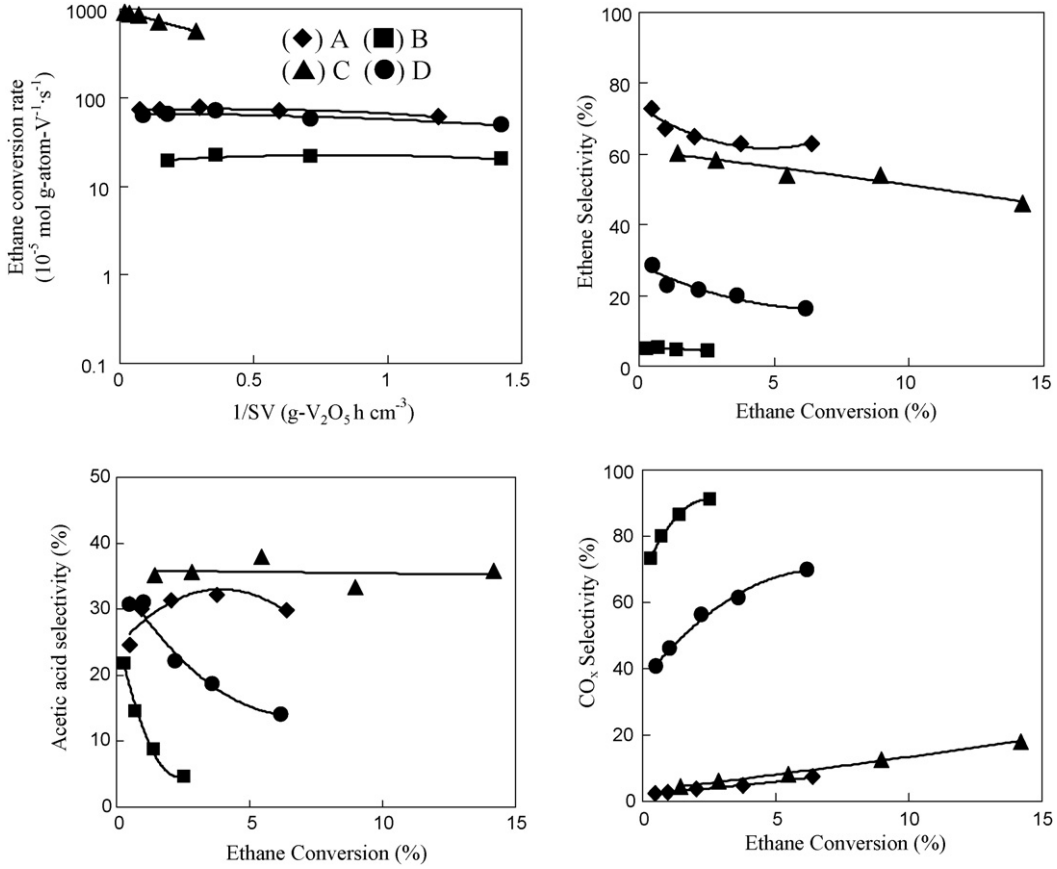

Fig. 5. Ethane oxidation on (A) $Mo_{0.61}V_{0.31}Nb_{0.08}O_x$; (B) $Mo_{0.61}V_{0.31}Nb_{0.08}O_x/ZrO_2$; (C) $Mo_{0.61}V_{0.31}Nb_{0.08}O_x/TiO_2$ and (D) $Mo_{0.61}V_{0.31}Nb_{0.08}O_x/Al_2O_3$ at 573 K. Partial pressures: ethane, 533 kPa; O_2, 107 kPa; H_2O, 320 kPa; He, 629 kPa; N_2, 11 kPa.

diffraction patterns (Fig. 1) and by the presence of Raman features assigned to Mo_5O_{14}-like species (Fig. 2). The presence of low-valent metal cations in both samples was evident from pre-edge absorption features in their UV–vis spectra (Fig. 3).

The precipitation of active $Mo_{0.61}V_{0.31}Nb_{0.08}O_x$ structures in the presence of colloidal dispersion of Al_2O_3, however, gave similar ethane conversion rates (per V-atom) as bulk $Mo_{0.61}V_{0.31}Nb_{0.08}O_x$ catalysts, but much higher CO_x selectivities (40–70%) than on unsupported catalysts. CO_x selectivities increased and ethene and acetic acid selectivities concurrently decreased with increasing residence time, indicating that unselective structures formed by interactions between $Mo_{0.61}V_{0.31}Nb_{0.08}O_x$ and Al_2O_3 surfaces catalyzed oxidation of ethene or acetic acid to CO and CO_2 (Fig. 5). $Mo_{0.61}V_{0.31}Nb_{0.08}O_x/ZrO_2$ catalysts gave lower ethane oxidation rates (per V-atom) than unsupported powders, despite their higher total (260 $m^2\ g^{-1}$) and Mo-V-Nb oxide (234 $m^2\ g^{-1}$) areas relative to unsupported powders (7.8 $m^2\ g^{-1}$). ZrO_2-containing catalysts gave even higher CO_x selectivities than $Mo_{0.61}V_{0.31}Nb_{0.08}O_x/Al_2O_3$. (Fig. 5). Low-valent metal cations, prevalent in bulk and TiO_2-containing samples, were not detected in the UV–vis spectra of Al_2O_3- or ZrO_2-supported samples (Fig. 3). These kinetic and structural evidence shows that oxide structures formed in the presence of Al_2O_3 or ZrO_2 suspensions differ from those on bulk oxides and appear to implicate an essential role of Mo_5O_{14} structures in selective catalysis. Previous studies have claimed that the unstable nature of Mo_5O_{14} leads to facile reduction and cation/anion diffusion and high reactivity for oxidations proceeding via Mars van Krevelen redox cyles [37].

These data show that TiO_2 colloids favor the formation of active structures with higher dispersion than on unsupported catalysts without forming unselective linkages between active oxides and support surfaces or other unselective or inactive structures. Ethane oxidation on $Mo_{0.61}V_{0.31}Nb_{0.08}O_x$ and $Mo_{0.61}V_{0.31}Nb_{0.08}O_x/TiO_2$ gave only 30–40% acetic acid selectivity and >50% ethene selectivity. Thus, it appears that higher acetic acid selectivities require the incorporation of catalytic functions for ethene oxidation to acetic acid. We discuss this below, immediately after an intervening description of the role of V and Mo components in mixed oxides in catalyzing the various steps relevant to the synthesis of acetic acid from ethane.

3.4. The role of vanadium and molybdenum oxide components in supported catalysts for ethane oxidation to acetic acid

Dispersed VO_x domains are the most effective catalysts for oxidative dehydrogenation (ODH) of alkanes [38], because they catalyze kinetically relevant C–H bond activation steps more effectively than less reducible MoO_x, WO_x and NbO_x domains of similar size [39,40]. The reactivity of supported VO_x domains in alkane ODH reactions increases with size because of a concomitant increase in the reducibility of active V centers [39].

We examine here well-dispersed VO_x, MoO_x, and VO_x-MoO_x domains to determine whether they can provide the required catalytic functions for ethane conversion to acetic acid. VO_x/TiO_2 catalyzes these reactions at the conditions used above for bulk and supported Mo-V-Nb oxide catalysts (Table 4), but with much higher CO_x selectivity (62%) than Mo-V-Nb oxides (<5%) at the same ethane conversion. The high CO_x selectivities of dispersed VO_x domains appear to be related to the presence of exposed support surfaces or unselective V-O-Ti linkages, which catalyze unselective ethene and acetic acid oxidation to CO_x [23]. The slightly higher VO_x domains density (14.5 V nm^{-2}) as well as the presence of MoO_x in $Mo_{0.61}V_{0.31}Nb_{0.08}O_x/TiO_2$ catalyst led to a marked decrease in the number of exposed V-O-Ti or Ti-O-Ti linkages. In contrast, MoO_x/TiO_2 gave nearly undetectable ethane oxidation rates. These data indicate that VO_x species within monovanadate or two-dimensional polyvanadate structures catalyze all steps required to form acetic acid from ethane, albeit less effectively and with greater contributions from unselective combustion pathways. The presence of MoO_x in VO_x/TiO_2 catalysts led to slightly higher ethene and acetic acid selectivities, apparently because MoO_x species titrate unselective Ti-O-Ti or V-O-Ti sites and form more selective but less reducible V-O-Mo linkages. The less reducible nature of VO_x structures when modified by MoO_x is consistent with its higher edge energy in the UV–vis spectrum [23].

3.5. PdO_x species as co-catalysts for the oxidation of ethene to acetic acid

$Mo_{0.61}V_{0.31}Nb_{0.08}O_x/TiO_2$ and $Mo_{0.61}V_{0.31}Nb_{0.08}O_x$ catalysts give similar amounts of ethene and acetic acid, because ethene oxidation to acetic acid in secondary reactions is relatively slow. This kinetic hurdle limits acetic acid synthesis rates and selectivities and increases the probability that reactive ethene intermediates convert to undesired CO_x products before being scavenged to more kinetically stable acetic acid products. The patent literature cites beneficial effects of metals (e.g. Pd, Au, Ag, Ir co-precipitated with active oxides) on acetic acid selectivity [17–20,41,42], without unequivocal mechanistic interpretations. Pd was chosen in the present study, because of

Table 4
Ethane oxidation on highly dispersed VO_x, MoO_x and MoO_x-VO_x catalysts

Catalyst	Ethane con. (%)	Selectivity (%)			Rate (10^{-5} mol g-atom-V^{-1} s^{-1})	
		Ethene	Acetic acid	CO_x	Ethene	Acetic acid
VO_x/TiO_2	1.0	27	11	62	450	54
MoO_x/TiO_2	1.2	14	6	80	61	4
MoO_x-VO_x/TiO_2	1.0	28	16	56	463	91

Reaction conditions: temperature, 573 K; partial pressure: ethane, 533 kPa; O_2, 107 kPa; H_2O, 320 kPa; He, 629 kPa and N_2, 11 kPa.

Table 5
Promoting effect of PdO_x for acetic acid synthesis from ethane oxidation on TiO_2-supported Mo-V-Nb oxides

Catalyst	Ethane con. (%)	Selectivity (%)			Rate (10^{-5} mol g-atom-V^{-1} s^{-1})	
		Ethene	Acetic acid	CO_x	Ethene	Acetic acid
$Mo_{0.61}V_{0.31}Nb_{0.08}O_x/TiO_2$	5.4	58	35	7	470	310
0.01% $Pd/Mo_{0.61}V_{0.31}Nb_{0.08}O_x/TiO_2$	5.1	1	82	17	7	650
0.005% $Pd/Mo_{0.61}V_{0.31}Nb_{0.08}O_x/TiO_2$	5.1	3	77	21	21	620
0.0025% $Pd/Mo_{0.61}V_{0.31}Nb_{0.08}O_x/TiO_2$	4.6	5	78	16	38	550

Reaction conditions: temperature, 573 K; partial pressure: ethane, 533 kPa; O_2, 107 kPa; H_2O, 320 kPa; He, 629 kPa and N_2, 11 kPa.

its prevalent use in ethene oxidation to acetaldehyde as homogeneous $PdCl_2$-$CuCl_2$ catalysts [43] and as their heterogeneous analogs (PdO_x-V_2O_5) [44–46].

Previous approaches that introduce PdO_x during co-precipitation lead to inefficient use of Pd atoms, because of their distribution throughout inaccessible locations within large oxide crystallites. These co-precipitation methods also prevent systematic variations of the type and amount of the Pd-based component and a rigorous assessment of the specific role of PdO_x in acetic acid synthesis. The use of physical mixtures of active Mo-V-Nb oxides and pre-formed Pd-based catalysts allows us to vary the contributions of PdO_x components, without concurrent changes in their accessibility or structure. Here, PdO_x was introduced as a separate 0.3 wt.% Pd/SiO_2 component in a physical mixture with $Mo_{0.61}V_{0.31}Nb_{0.08}O_x/TiO_2$ samples.

Ethane oxidation on 0.01 wt.% $Pd/Mo_{0.61}V_{0.31}Nb_{0.08}O_x/TiO_2$ gave higher acetic acid formation rates (6.5×10^{-3} mol g-atom-V^{-1} s^{-1}) than $Mo_{0.61}V_{0.31}Nb_{0.08}O_x/TiO_2$ (3.1×10^{-3} mol g-atom-V^{-1} s^{-1}). Ethene was nearly depleted from the reactor effluent (net ethene formation rates decreased from 4.7 to 0.07×10^{-3} mol g-atom-V^{-1} s^{-1}) when 0.01 wt.% Pd present in $Mo_{0.61}V_{0.31}Nb_{0.08}O_x/TiO_2$ (Table 5). The presence of the Pd-based co-catalyst did not influence ethane oxidation rates, but markedly increased acetic acid synthesis rates by merely converting ethene intermediates to acetic acid. Acetic acid selectivities increased from ~35 to ~82% (Table 5; 5% ethane conversion), while ethene selectivities decreased from ~58 to ~1%. This catalyst mixture gave acetic acid productivities more than two-fold higher (>800 g/kg-cat-h) than on the best catalysts previously reported ($Mo_1V_{0.36}Nb_{0.03}Sb_{0.01}Ca_{0.01}Pd_{0.0005}$ (410 g/kg-cat-h) at similar reaction conditions [19] (Table 1).

We have previously shown [4] that during ethene oxidation Pd increased only the rate of ethene oxidation to acetaldehyde, while active Mo-V-Nb oxides in physical mixtures scavenge acetaldehyde to form acetic acid before its sequential oxidation to CO_x. In contrast, Pd/SiO_2 by itself forms predominantly CO_x (80% CO_x; 3–12% ethene conversion) from ethene-O_2 reactants. Acetaldehyde reacts rapidly on Mo-V-Nb oxides to form acetic acid, a less reactive molecule in oxidation reactions. These fast catalytic pathways and the intermediate role of acetaldehyde have been demonstrated from the effects of residence time during oxidation of ethene [4] and ethanol [8] on these catalysts. These data provide evidence for the mutually synergistic effects of the Pd and Mo-V-Nb oxide functions, which is also evident in the reactions of ethene intermediates during ethane conversion to acetic acid. We conclude that atomic proximity between Pd and active metal oxides is not required because ethene intermediates can diffuse between the two catalytic functions. We also show that samples with 0.01% Pd in these physical mixtures are sufficient to nearly deplete ethene intermediates and to covert them selectively to acetic acid. Indeed, Pd contents even as low as 0.0025 wt.% in these physical mixtures also led to near depletion of ethene intermediates (Table 5). We note that the presence of Pd increases only slightly the CO_x selectivity; the observed absence of secondary combustion pathways appears to reflect the presence of PdO_x species as small clusters, which are much less reactive than larger PdO_x structures in catalytic combustion of hydrocarbons [47,48].

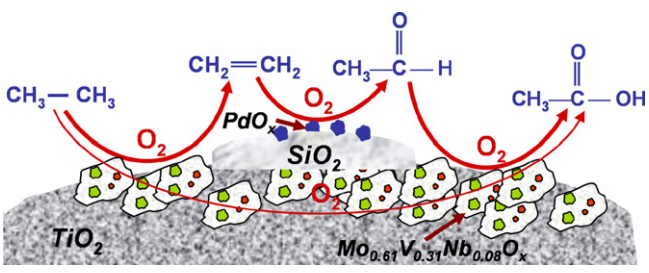

Scheme 1. Possible reaction pathways of ethane oxidation to acetic acid.

The mechanistic basis for the catalytic improvements demonstrated here for ethane oxidation to acetic acid on Mo-V-Nb oxides is illustrated in Scheme 1. A significantly higher dispersion of active $Mo_{0.61}V_{0.31}Nb_{0.08}O_x$ components was achieved by their precipitation in the presence of colloidal TiO_2 without the concomitant introduction of unselective catalytic sites. The secondary oxidation of ethene to acetic acid was catalyzed by a second function, provided by small PdO_x clusters effective even when present as a physical mixture with $Mo_{0.61}V_{0.31}Nb_{0.08}O_x$ catalysts. PdO_x clusters catalyze ethene oxidation to acetaldehyde, but $Mo_{0.61}V_{0.31}Nb_{0.08}O_x$ sites are required to scavenging acetaldehyde to form acetic acid, which is less likely to convert to CO_x than reactive acetaldehyde molecules.

4. Conclusions

The catalytic activity of ethane oxidation to ethene and acetic acid on multi-component oxide, $Mo_{0.61}V_{0.31}Nb_{0.08}O_x$, was enhanced by the structural dispersion of active oxides on

TiO_2; more than 10 times higher reaction rates were achieved with similar selectivities to all the products, ethene, acetic acid and CO_x. However, negative effects were observed when supporting on Al_2O_3 and ZrO_2 because of the introduction of unselective linkages which encouraged the combustion reactions of ethene and/or acetic acid. The similar formation rates of ethene and acetic acid during ethane oxidation indicated the slow conversion of ethene to acetic acid on Mo-V-Nb oxides. This kinetic hurdle limits acetic acid synthesis rates and selectivities were overcome by physically mixing with Pd/SiO_2 ($Pd \leq 0.01$ wt.%), which increased markedly the oxidation rate of ethene to acetaldehyde and nearly depleted ethene intermediates during the reaction; acetaldehyde was then oxidized to acetic acid rapidly on $Mo_{0.61}V_{0.31}Nb_{0.08}O_x$. VO_x domains as dispersed structures on TiO_2 catalyze all of the steps required for the formation of acetic acid, but favor total combustion reactions to CO_x; The exposed support surface or the linkage of support and active component are believed to be responsible for the high CO_x selectivity when reaction performed on the highly dispersed materials. MoO_x domains, however, are essentially unreactive for ethane oxidation.

Acknowledgements

We acknowledge with thanks the financial support by ExxonMobil Research and Engineering Co. and helpful technical discussions with Dr. Nan Yao.

Appendix A. Supplementary data

Supplementary data associated with this article can be found, in the online version, at doi:10.1016/j.apcata.2007.10.021.

References

[1] F.E. Paulik, J.F. Roth, Chem. Commun. (1968) 1578.
[2] E.M. Thorsteinson, T.P. Wilson, F.G. Young, P.H. Kasai, J. Catal. 52 (1978) 116.
[3] K.I. Sano, H. Uchida, S. Wakabayashi, Catal. Surv. Jpn. 3 (1999) 55.
[4] X. Li, E. Iglesia, Angew. Chem. Int. Ed. 46 (2007) 8649.
[5] C.H. Christensen, B. Jøgensen, J. Rass-Hansen, K. Egeblad, R. Madsen, S.K. Klitgaard, S.M. Hansen, M.R. Hansen, H.C. Andersen, A. Riisager, Angew. Chem. 118 (2006) 4764, Angew. Chem. Int. Ed. 45 (2006) 4648.
[6] F. Gonçalves, P.R.S. Medeiros, J.G. Eon, L.G. Appel, Appl. Catal. A 193 (2000) 195.
[7] M. Gubelmann-Bonneau, US 5,840,971 (1998).
[8] X. Li, E. Iglesia, Chem. Eur. J. 13 (2007) 9324.
[9] M. Roy, M. Gubelmann-Bonneau, H. Ponceblanc, J.C. Volta, Catal. Lett. 42 (1996) 93.
[10] M. Roy, H. Ponceblanc, J.C. Volta, Top. Catal. 11/12 (2000) 101.
[11] L. Tessier, E. Bordes, M. Gubelmann-Bonneau, Catal. Today 24 (1995) 335.
[12] A.H. Fakeeha, Y.M. Fahmy, M.A. Soliman, S.M. Alwahabi, J. Chem. Technol. Biotechnol. 75 (2000) 1160.
[13] M. Sopa, A. Waclaw-Held, M. Grossy, J. Pijanka, K. Nowinska, Appl. Catal. A 285 (2005) 119.
[14] E. Bordes, L. Tessier, M. Gubelmann-Bonneau, European Patent Application EP 683,153.
[15] J.H. Holles, C.J. Dillon, J.A. Labinger, M.E. Davis, J. Catal. 218 (2003) 42.
[16] J.M. Galownia, A.P. Wight, A. Blanca, J.A. Labinger, M.E. Davis, J. Catal. 236 (2005) 356.
[17] M. Kitson, EP 407,091 (1990).
[18] K. Karim, M. Al-Hazmi, A. Khan, US 6,060,421 (2000).
[19] H. Borchert, U. Dingerdissen, DE 19,745,902 (1997).
[20] B.I. Rosen, WO 2,004,067,167 (2004).
[21] J.F. Brazdil, R.J. George, B.I. Rosen, WO 2,005,018,804 (2005).
[22] A. Khodakov, J. Yang, S. Su, E. Iglesia, A.T. Bell, J. Catal. 177 (1998) 343.
[23] S. Yang, E. Iglesia, A.T. Bell, J. Phys. Chem. B 109 (2005) 8987.
[24] G. Centi, Appl. Catal. A 147 (1996) 267.
[25] F. Prinetto, G. Cerrato, G. Ghiotti, A. Chiorino, M.C. Campa, D. Gazzoli, V. Indovina, J. Phys. Chem. 99 (1995) 5556.
[26] D.G. Barton, M. Shtein, R.D. Wilson, S.L. Soled, E. Iglesia, J. Phys. Chem. B 103 (1999) 630.
[27] S. Rondon, M. Houalla, D.M. Hercules, Surf. Interface Anal. 26 (1998) 329.
[28] D. Linke, D. Wolf, M. Baerns, O. Timpe, R. Schlögl, S. Zeyß, U. Dingerdissen, J. Catal. 205 (2002) 16.
[29] M. Dieterle, G. Mestl, J. Jäger, Y. Uchida, H. Hibst, R. Schlögl, J. Mol. Catal. A: Chem. 174 (2001) 169.
[30] L. Kihlborg, Ark. Kemi 21 (1963) 427.
[31] N. Yamazoe, L. Kihlborg, Acta Cryst. B 31 (1975) 1666.
[32] M. Roussel, M. Bouchard, E. Bordes-Richard, K. Karim, S. Al-Sayari, Catal. Today 99 (2005) 77.
[33] B. Olthof, A. Khodakov, A.T. Bell, E. Iglesia, J. Phys. Chem. B 104 (2000) 1516.
[34] I.E. Wachs, Catal. Today 27 (1996) 437.
[35] P. Concepcíon, P. Botella, J.M. López Nieto, Appl. Catal., A 278 (2004) 45.
[36] K. Ruth, R. Burch, R. Kieffer, J. Catal. 175 (1998) 27.
[37] G. Mestl, Ch. Linsmeier, R. Gottschall, M. Dieterle, J. Find, D. Herein, J. Jäger, Y. Uchida, R. Schlögl, J. Mol. Catal. A: Chem. 162 (2000) 463.
[38] H.H. Kung, Adv. Catal. 40 (1994) 1.
[39] K.D. Chen, A.T. Bell, E. Iglesia, J. Phys. Chem. B 104 (2000) 1292.
[40] K. Chen, A.T. Bell, E. Iglesia, J. Catal. 209 (2002) 35.
[41] B. Ellis, M.D. Jones, EP 1,043,064 (2000).
[42] B. Ellis, J. Cook, M.D. Jones, S.J. Kitchen, P. Howard, WO 9,951,339 (1999).
[43] J.R. Smidt, W. Hafner, R. Jira, J. Sedlmeier, R. Sieber, R. Ruttinger, H. Kojer, Angew. Chem. 71 (1959) 176.
[44] A.B. Evnin, J.A. Rabo, P.H. Kasai, J. Catal. 30 (1973) 109.
[45] J.L. Seoane, P. Boutry, R. Montarnal, J. Catal. 63 (1980) 182.
[46] J.L. Seoane, P. Boutry, R. Montarnal, J. Catal. 63 (1980) 191.
[47] A. Ali, W. Alvarez, C.J. Loughran, D.E. Resasco, Appl. Catal. B 14 (1997) 13.
[48] J.G. McCarty, Catal. Today 26 (1995) 283.